PERGAMON

Electrochimica Acta 44 (1999) 3865–3883

ELECTROCHIMICA Acta

Passivation and corrosion of microelectrode arrays

G. Schmitt[a,*], J.-W. Schultze[b], F. Faßbender[c], G. Buß[b], H. Lüth[d], M.J. Schöning[d]

[a]*Laboratory for Corrosion Protection, Iserlohn University of Applied Science, 58590 Iserlohn, Germany*
[b]*Institut für Physikalische Chemie und Elektrochemie, Heinrich-Heine-Universität Düsseldorf, Düsseldorf, Germany*
[c]*Institute for Technical Chemistry and Petroleum Chemistry, Aachen University of Technology, Aachen, Germany*
[d]*Institute of Thin Film and Ion Technology, Forschungszentrum Jülich GmbH, Jülich, Germany*

Received 9 September 1998; received in revised form 14 January 1999

Abstract

Application of silicon based microsensors in electrolyte solutions is hampered by insufficient barrier properties and poor corrosion resistance of common passivation layers used to protect the underlying conducting tracks and microelectronic structures. Therefore, the protectivity of various types of compatible passivation layers (organic polyimide and photoresist films, inorganic mono, duplex and triplex layers based on PECVD silicon oxide and silicon nitride) was investigated and improved on microelectrode arrays exposed to 1 M NaCl (pH 2 to 10) at 25°C. Duplex SiO_2/Si_3N_4 and oxide/nitride/oxide (ONO) triplex layers with optimised nitride PECVD process yielded the best barrier properties. Burying the conducting tracks in the thermal silicon oxide layer improves the performance significantly. Failures of the passivation layers, detected by leak current and layer resistance measurements with subsequent SEM investigation, result from cracking due to intrinsic and extrinsic (less important) mechanical stress, film defects (pinholes, particle inclusions), from chemical, physicochemical and electrochemical reactions (external, internal, sublayer corrosion) and from the combined action of mechanical stress and chemical interaction (stress corrosion cracking).

Keywords: Corrosion; PECVD SiO_2; PECVD Si_3N_4; Passivation layer; Microelectrode array; Sensor chips

1. Introduction

In recent years the microsystem technology has gained increasing importance due to exciting and extraordinary developments in the field of sensors, actuators and micromechanical tools. Miniplants have been designed and prepared aiming at miniaturising production plants into the liter, milliliter and even microliter scale [1]. A powerful microsystem technology needs, however, a great variety of different miniaturised sensors to cope with the requirements of integrated analytical, monitoring and process control systems.

Miniaturisation of sensors down to the micrometer scale is easily achieved using the well established methods in silicon planar technology [2]. Microsensors exhibit a wide application potential [3] ranging from medical diagnosis, biotechnology and biological research, over food control to environmental monitoring [4].

However, the application of these silicon based sensors is severely hampered by the fact that the sensors generally fail too fast (within minutes or only a few hours) when used in liquid media, specifically in elec-

* Corresponding author. Tel.: +49-23-71-160.
E-mail address: schmitt.g@mfh-iserlohn.de (G. Schmitt)

0013-4686/99/$ - see front matter
PII: S0013-4686(99)00094-8

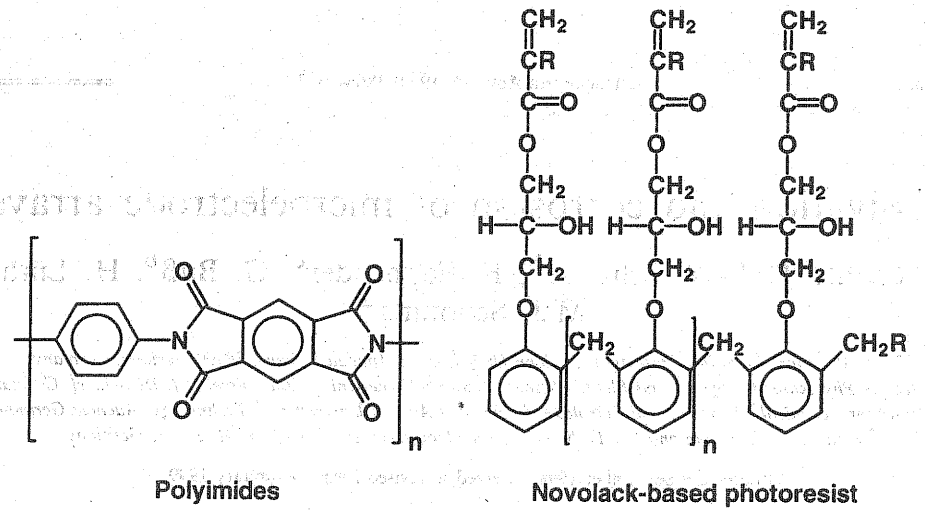

Fig. 1. Chemical structures of organic passivation films.

trolyte solutions. This is due to the poor barrier efficiency of the passivation layers (thickness 0.25 to 1 μm) generally used to insulate conducting tracks and integrated functional microelectronic devices on the chip. Passivation layers also provide scratch and particle protection to the circuit chip during mounting, bonding and packaging. The poor performance of the passivation layers relates to the fact that they were originally developed and optimised to serve as dielectrics in clean, noncorrosive environments. Exposure to liquid media was not intended and/or anticipated. On the contrary, microelectronic chips are very often hermetically encapsulated to protect from environmental degradation, e.g. by moisture and/or electrolytes.

To open the potential multitude of applications to silicon based microsensors, it is, therefore, a precondition to increase the barrier performance of passivation layers considerably. Thus, in a multidisciplinary approach the authors investigated and optimised the protective properties of different types of passivation layers using a versatile microelectrode array as an investigation tool.

2. Passivation layers

2.1. Chemical nature

Passivation layers can be organic and inorganic in nature. Organic passivation layers can consist of polyimides as well as photoresist laquers. While polyimides are formed by polycondensation reactions of (generally aromatic) polycarboxylic acids (e.g. pyromellitic anhydride) and (generally aromatic) polyamines (e.g. *p*-phenylene diamine) (Fig. 1), the photoresist films are quite often novolack-based and formed by polycondensation of phenolic compounds (e.g. phenol, bisphenol A) with formaldehyde and subsequent reaction with unsaturated epoxi esters of the acrylic type (Fig. 1). The organic passivation layers are generally applied by spin coating processes.

Inorganic passivation layers include silicon dioxide (SiO_2), silicon nitride (Si_3N_4), silicon oxinitride ($Si_xO_yN_z$,) and silicon carbide (SiC). They are applied as mono layers, duplex layers (e.g. SiO_2/Si_3N_4) or triplex layers (e.g. oxide/nitride/oxide (ONO) layers in the sequence $Si0_2/Si_3N_4/SiO_2$).

These layers are generally prepared by plasma-enhanced chemical vapour deposition (PECVD) via decomposition of appropriate gas mixtures. Gases introducing silicon include silane (SiH_4), chlorosilanes (e.g. SiH_2Cl_2, $SiCl_4$) and low molecular weight siloxanes (e.g. $Si(OC_2H_5)_4$). Oxides are formed in the presence of oxygen and/or dinitrogen oxide (N_2O). The nitrogen in the nitrides can stem from additions of, for example, ammonia (NH_3), nitrogen (N_2), N_2O or nitrogen trifloride (NF_3).

Due to the specific deposition method which uses glow discharge to form reactive species like ions, excited molecules and radicals from the gas components, the PECVD layers are composed of stoichiometric compounds like SiO_2, Si_3N_4 or SiC only in the ideal case. Real PECVD films consist of non-stoichiometric compounds containing varying amounts of other elements (hydrogen, chlorine or fluorine) depending on the specific deposition conditions [5], e.g. the nature and concentration of reactive gases in the gas mixture, the temperature, the total pressure, the gas

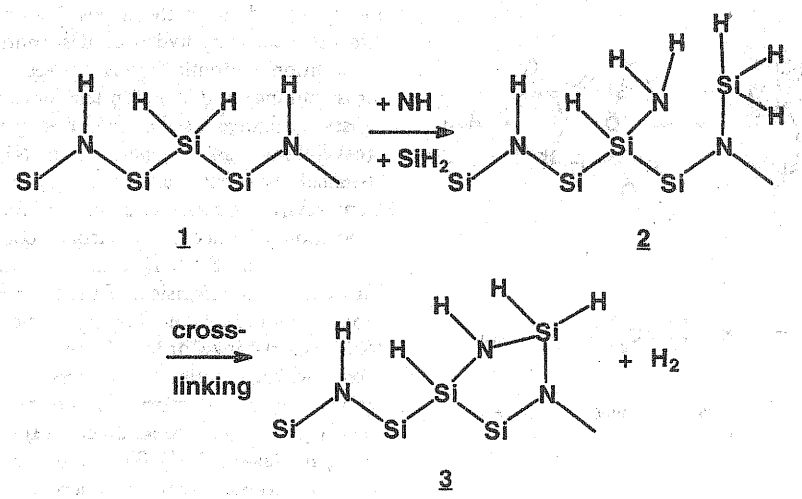

Fig. 2. Growth reaction (1 ⇒ 2) and cross-linking reaction (2 ⇒ 3) during deposition of plasma Si–N [5].

flow and the plasma (glow discharge) conditions (RF frequency range).

Thus, PECVD silicon nitride layers can contain Si–H and N–H bonds as schematically shown in Fig. 2 [5]. Under glow discharge conditions active species such as ions, excited molecules and radicals are formed by electron impact of relatively stable molecules, resulting in a very complex reaction system, which at the end yields the plasma silicon nitride layer.

The most important intermediates in the gas phase of SiH_4/NH_3–N_2 mixtures are the SiH_2 and NH radicals [5]. Eqs. (1) and (2) show primary reaction steps with these radicals.

$$SiH_2 + SiH_4 \rightarrow Si_2H_6 \quad (1)$$

$$SiH_2 + NH \rightarrow SiNH_3 \quad (2)$$

Radical chain reactions finally form silazane chains (Fig. 2). Cross-linking occurs by hydrogen elimination. As this reaction is temperature-dependent, the hydrogen content of plasma SiN deposits can vary between 10 and 40 at% [6,7]. At high Si/N ratios (Si rich layers with $Si/N \approx 1.4$) almost all hydrogen is bonded to silicon. At Si/N ratios below 0.75, most of the hydrogen is bonded to nitrogen [5]. Plasma SiN layers could be best described as polysilazane ($Si_xH_yN_z$), i.e. as an inorganic polymer [7].

Plasma SiO_2 may contain 5 to 10 at% hydrogen, all bonded as OH [7].

Post-treatment of PECVD layers with reactive gases (CF_4, HCF_3, oxygen plasma, etc.) can change the chemical nature and composition in near-surface zones up to depths of several tenth of nanometers.

2.2. Physical properties

The non-stoichiometry of the layer composition influences the density, the mechanical properties (Young's modulus, ultimate tensile stress, microhardness, intrinsic growth stress, fracture stress, fracture strain), the electrical properties [6] (electrical resistance, permittivity) and the growth structure [8] of the passivation layers.

In the following, the mechanical properties and growth structures of inorganic passivation layers shall be discussed in more detail, as they directly influence their performance under corrosive environmental conditions. Thus, films in tension tend to develop cracks, whereas those with high compressive stress tend to delaminate and peel off. The stress state of the dielectric can also affect the metal layers it isolates. It is known that intrinsic stresses in plasma SiN passivation layers can have tremendous influence on the stress induced voiding as well as hillock growth on aluminium runners in double level metal integrated circuits [9]. Lowering the residual stress of the film is also desirable to prevent the underlying aluminium film from notching [9].

Depending on the deposition conditions the mechanical properties of plasma passivation layers can vary within broad limits. This has been widely investigated during recent years.

2.2.1. Silicon dioxide

Plasma SiO_2 layers are generally produced with compressive stresses in the range from 0.5 to $5–10^8$ Pa [10–12]. Reports on tensile stress in such films are scarce

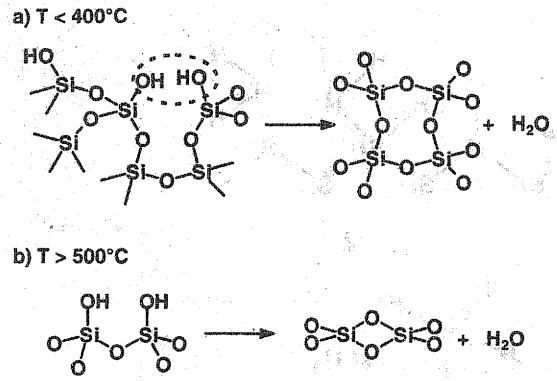

Fig. 3. Dehydroxylation of silica to produce (a) silicate rings or (b) edgeshared tetrahedra [56].

[13]. The compressive stress in plasma SiO_2 layers is due to the mismatch of the thermal expansion coefficients of the film and the silicon substrate [10]. The compressive stress decreases with increasing OH concentration in the layer [10,11]. However, with increasing OH concentration the porosity of the film increases which is not desirable in view of its function as a corrosion barrier layer.

Stress in plasma SiO_2 films can be influenced by the deposition parameters [14,15,16,17]. If plasma SiO_2 films absorb moisture they can become more compressive with storage time [18,19]. High Si–O–Si bond strain and incorporated impurities are responsible for the instability of film stress during post-deposition aging [20]. After exposition to ambient conditions, the strained Si–O bonds react with moisture and convert to neighbour silanol groups (Si–O–H). Due to silanol formation, the film expands or swells and gives rise to increased compressive stress.

The stress can be influenced by post-deposition annealing [21–27]. Subsequent annealing of these films at temperatures above 250°C causes near-neighbour silanol groups to react. Release of water produces a reconstructed Si–0 network [26] (Fig. 3). The strain in the newly formed Si–0 bonds is much less than the strain of the original Si–0 bonds. Thus, annealing can considerably improve the film quality. The largest improvement can be achieved by annealing in the presence of steam. However, depending on the annealing conditions, the films can also assume a high tensile stress which can cause, among other things, void formation in Al interconnects. Annealing at temperatures below the densification temperature can make SiO_2 films more porous [27].

2.2.2. Silicon nitride

Plasma Si–N layers can exhibit compressive stresses up to -12×10^8 Pa and tensile stresses up to 6×10^8 Pa [5] depending on the deposition conditions. Tensile stress is created by hydrogen desorption and formation of additional atomic bonds between Si and nitrogen (cross-linking) at deposition temperature (Fig. 2) which causes shrinkage of the film. For low Si–NH_3 ratios cross-linking can originate from NH_3 evolution by chemical condensation reaction of $Si(NH_2)_3$ [28]. Compressive stress is due to ion bombardment (after deposition of silicon- or nitrogen-containing radicals) on the growing Si–N layer at deposition temperature. This causes an expansion of the layer due to implanted atoms and broken Si–N bonds which leads to a distorted short-range order of the Si–N-structure [5]. A model which correlates film stress to that contributed by (1) lattice distortion induced by Si–H and N–H bondings, (2) ion bombardment, (3) thermal mismatch between plasma Si–N films and the silicon substrate and (4) intrinsic stress introduced during formation of covalent Si–N bonding is proposed and examined in Ref. [9].

The cracking resistance (CR) of thick (approximately 1 μm) Si–N films at a given temperature T is functionally related to its density ρ, intrinsic stress σ_i, thermal mismatch Δ_α with the silicon substrate and deposition temperature T_s through the following equation [8,29]:

$$\mathrm{CR} = \frac{\rho}{\rho_0} \times \sigma_u - \sigma_i - \frac{E}{1-\nu} \int_{T_s}^{T} \Delta_\alpha \, \mathrm{d}T \qquad (3)$$

where σ_u is the ultimate tensile stress of the structurally 'perfect' CVD-Si_3N_4 film with the density ρ_0 and E and ν are the Young's modulus and Poisson's ratio for the film. This equation correctly predicts that CR will be improved if ρ is increased, σ_i and Δ_α are made small and T_s is made high relative to the test temperature. A quantitative application of the above equation, including thermal stress measurements, for various plasma Si–N films are described in Ref. [30]. Experimental results relating the composition, density and mechanical stress of plasma Si–N layers are given in Refs. [5,9,10,31,32,33,34,35].

Intrinsic stress in as-deposited plasma Si–N films can be changed by follow-on processing, e.g. by ion implantation and annealing [18,36,37,38,39].

Depending on the deposition process parameters the physical properties of plasma Si–N will range within some limits [40], e.g. the Young's modulus E: 85–210 GPa [41,42], the density ρ: 2.3–3.1 g/cm^3 [5,18,43], the refractive index n: 1.8–2.6 [18,43–45], the resistivity: 10^4–10^{20} Ω cm at 2×10^6 V/cm, depending on the Si/N ratio [8,43,46], the dielectric constant ε: 6–8 at 1 MHz [8,42,43,]), the breakdown strength: $1–5 \times 10^6$ V cm^{-1} [36,45]. The Poisson ratio ν was found to be 0.25 [42] and the expansion coefficient α was given to be 1.5×10^{-6} °C^{-1} [47].

Table 1
Failure modes of passivation layers

Group	Failure Mode	Schematic Sketch
1	**Failures due to mechanical stress and film defects**	
1.1 1.1.1 1.1.2	Cracks due to tensile stress intrinsic stress extrinsic stress	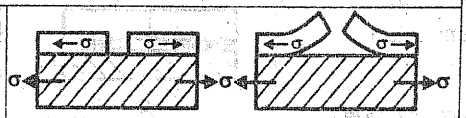
1.2 1.2.1 1.2.2	Cracks due to compressive stress intrinsic stress extrinsic stress	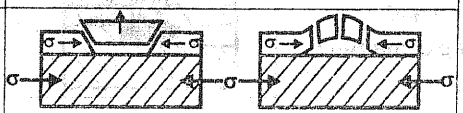
1.3 1.3.1 1.3.2	Cracks due to intrinsic stress induced by surface topography induced by swelling	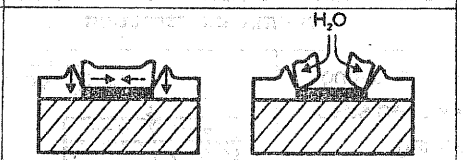
1.4	Pinholes	
1.5	Particle inclusion	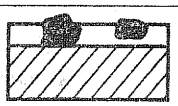
2	**Failures due to chemical, physicochemical and electrochemical reactions**	
2.1	Adsorption/Desorption processes	
2.2 2.2.1 2.2.2	external corrosion hydrolysis oxidation	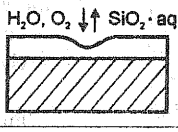
2.3	Absorption, Swelling	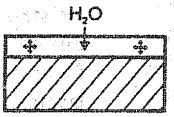
2.4	Diffusion processes	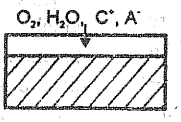

(continued on next page)

Table 1 (*continued*)

2.5 2.5.1 2.5.2	Internal corrosion hydrolysis oxidation	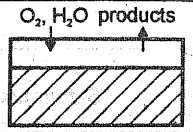
2.6 2.6.1 2.6.2	Sublayer corrosion without delamination with delamination	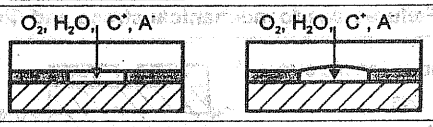
2.7	Sublayer corrosion due to easier swelling and hydrolysis of plasma Si-O	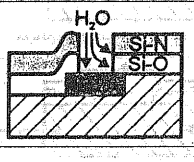
3	**Failures due to combined action of mechanical stress and chemical interaction**	
3.1	Stress corrosion cracking (Adsorption induced stress corrosion cracking)	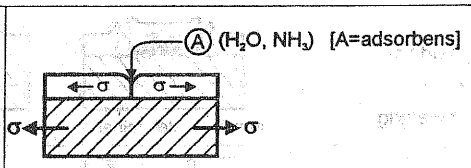

2.3. Structure and morphology

TEM (transmission electron microscope) investigations revealed that PECVD passivation films are amorphous. Detailed investigations on the crystallinity of plasma Si–N films are described in Ref. [8].

On properly cleaned device wafers a smooth layered growth structure is encountered. Nodular growth (formation of hillocks) generally indicates contaminated areas (e.g. sites with baked-on residues of photoresist and/or particulate matter) on device wafers, on conducting tracks and dielectric areas, respectively. The presence of such contaminations triggers a vapour–liquid–solid growth [48] and/or gas phase reactions [49] in the vicinity of the contaminated area. Such reactions in response to surface contamination were found to be more likely to occur under conditions of higher temperatures and larger gas flows during deposition which also leads to more crack-resistant layers [8]. Surface-activated film growth allows excellent step coverage, thus conforming well the underlying topology even where walls are vertical or have a slight negative slope [8]. The microstructure of the film can be correlated to its mechanical properties [9].

2.4. Failure mechanisms

The failure mechanisms of organic and inorganic passivation layers can be divided into three groups (Table 1):

Group 1: Failures due to mechanical stress and film defects.
Group 2: Failures due to chemical, physicochemical and electrochemical reactions.
Group 3: Failures due to the combined action of mechanical stress and chemical interactions.

Within group 1 cracking of passivation layers due to stresses, either extrinsic (externally applied) or intrinsic due to film growth, is a very important and common failure mode of inorganic and organic passivating layers.

Stress produces strain in the passivation layers which can lead to delamination, the intensity of which depends on the kind of stress and the adhesion of the film to the substrate. For a given layer there exists always a thickness-dependent critical strain, above which the layer cracks and may spall depending on the adhesion to the substrate and the ductility of the substrate. A general failure mode diagram for critical

strain ε_{crit} versus layer thickness h is given in Fig. 4 [50].

In the case of tensile stress only cracking of the film with no delamination or spalling will occur, if the film adhesion is good and the substrate exhibits a higher ductility than the film (Table 1, group 1.1a). Delamination and spalling will, however, occur if the film adhesion is poor, independent of the ductility ratio between film and substrate (Table 1, group 1.1b). In case of compressive stress the film will spall if its adhesion to the substrate is good (Table 1, group 1.2a), or will buckle if its adhesion is poor (Table 1, group 1.2b).

Stresses (generally intrinsic stresses) in passivating layers can be induced by the substrate topography, e.g. at edges of conducting tracks or other step structures, where the growth morphology of the film is more irregular and nodular growth is more likely to occur than on plain surfaces (Table 1, group 1.3).

While extrinsic tensile or compressive stresses can be avoided in passivating layers by appropriate design of the system in which a chip is integrated, it is much more complicated to avoid intrinsic stresses. It has been shown that in PECVD processes intrinsic stresses can be influenced by the deposition parameters [5,9]. It is possible to obtain stress-free silicon nitride films by a proper choice of process parameters under given boundary conditions. Boundary conditions are imposed, e.g. by the reactor which is available, i.e. the temperature range, RF frequency range, gas supply, etc., furthermore by the process compatibility and the film properties. Process compatibility can be an issue when high temperature processes follow the low temperature PECVD deposition of silicon nitride which can drastically change in morphology and intrinsic stress due to cross-linking processes (hydrogen desorption and formation of additional atomic bonds by cross-linking between Si and N (Fig. 2)).

The formation of pinholes (Table 1, group 1.4) is influenced by the parameters of the PECVD deposition process, e.g. the deposition temperature. Thus, for plasma Si–N the pinhole density is less than 1 pinhole per cm^2 for deposition temperatures above 300°C, while it is unacceptable high for deposition temperatures below 300°C [36].

Failures of passivation films due to particle inclusion (Table 1, group 1.5) is generally a matter of clean processing. This includes not only cleanliness in the rooms where the wafers are handled, but also in the PECVD chamber where particles of previous deposition processes could become attached to the chamber walls and fall onto a new wafer during the next passivation run. In this case the particle will be incorporated in the growing passivation film.

Group 2 failures include chemical, physicochemical and electrochemical reaction processes in their mechanisms. Adsorption of water via hydrogen bridging at hydrogen bonds at the surface of the film, e.g. Si–H, Si–O–H, Si–N–H, or at oxygen or nitrogen bonds, e.g. Si–O–Si or Si–N–Si, is an important first step for further chemical degradation of SiO_2 or Si–N films, e.g. by hydrolysis or by etching in hydrofluoric acid.

External corrosion of PECVD films, i.e. degrading the passivation layer from the surface, can be achieved by *hydrolysis* at different pH values. Acid hydrolysis is the degradation mechanism during etching. The etch rate, e.g. of plasma Si–N in 49% HF at 23°C is 150–300 nm/min [40]. The etch rate of plasma Si–N in buffered HF depends on the hydrogen content of the film [7] and, thus, on the deposition parameters [28] and ranges in the order 5–150 nm/min. The resistance of plasma SiN films against alkaline media is much higher. Thus, it was observed [44] that the etch rate in 30% KOH at 70°C is only 41 nm/h.

Oxidation of Si–N films in most environments (moist air, water vapour in the PECVD chamber) can occur by absorption of water with subsequent hydrolysis of Si–H bonds, thus introducing oxygen into the film (as Si–O–H groups) [37].

Absorption of small molecules (e.g. water molecules) in the film will cause swelling. This phenomenon can be observed both at organic and inorganic films. While swelling due to absorption processes is well known and has been extensively studied for organic films, there is awareness that also inorganic films can absorb and swell. Thus, plasma PECVD SiO_2 films can absorb

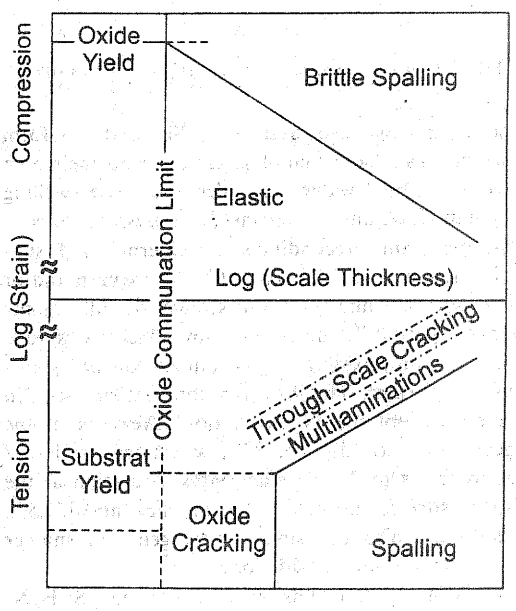

Fig. 4. Failure mode map for tensile and compressive strain [50].

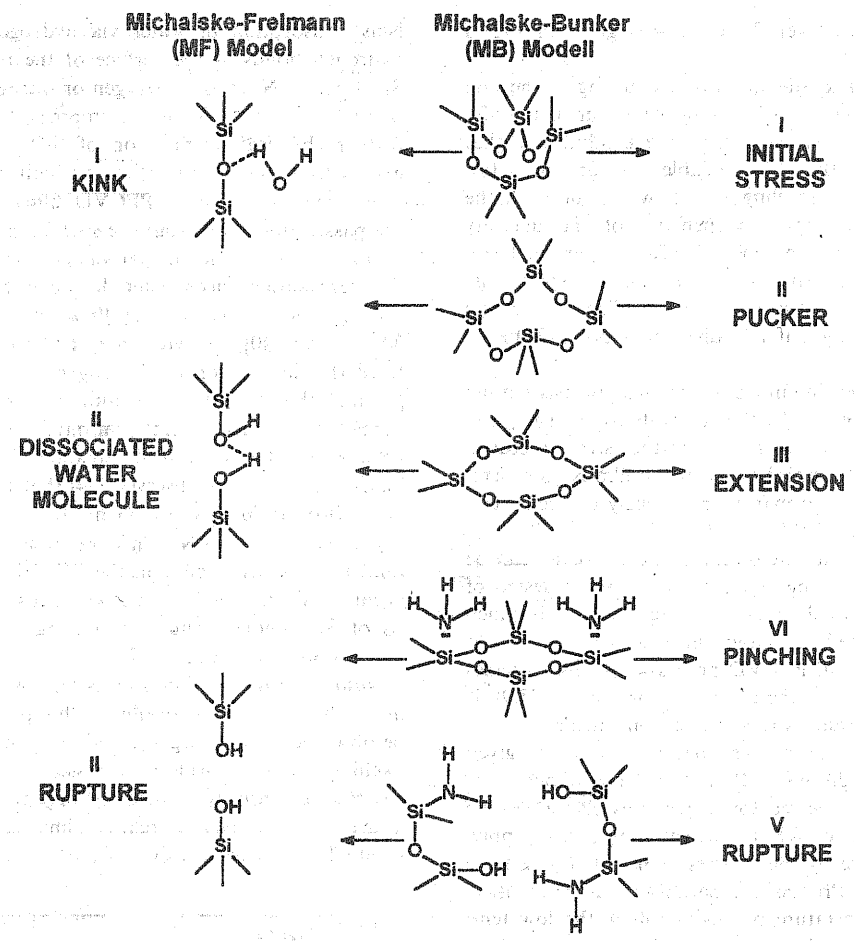

Fig. 5. Schematic diagrams of (a) MF amorphous silica model and (b) the MB amorphous silica fracture model [55,56,57].

water which may hydrolyse Si–O–Si bonds to form silanol groups. These silanol groups, due to their high polarity, can bind water molecules and cause swelling of the film increasing the intrinsic compressive stress.

An important precondition for internal and sublayer corrosion is the diffusion of water, oxygen and/or ions through the film. It is well known that all organic coatings, specifically those with low thicknesses (e.g. less than 1 μm), exhibit only a limited barrier against diffusion of water. The diffusion constant of water in polymers (acceptable as passivation layers) is in the range of 10^{-7} to 10^{-5} cm^2 s^{-1}, which means that it takes from 1 s to 2 h to reach 90% saturation at the substrate surface through a 25 μm thick film [51,52]. Polymers are also diffusible for oxygen and smaller ions, e.g. sodium or chloride ions.

For inorganic thin films such as SiO_2 and $Si_xH_yN_z$ the diffusion constant is several orders of magnitude less, reaching down to 10^{-18} cm^2 s^{-1} [51,52]. However, as mentioned above, e.g. plasma SiO_2 films can become more diffusible with increasing concentration of silanol groups, as these groups can bind water molecules and form domains with higher local water concentrations which allow diffusion of more water and ions. Thus, SiO_2 passivation films have only a limited barrier function for diffusion of sodium ions. In contrast to plasma SiO_2 films plasma Si–N layers provide some resistance to sodium ions and moisture permeation [53,54].

Absorption of water can lead to *internal corrosion by hydrolysis and oxidation*. Water reacts with strained Si–O or Si–N bonds and forms silanol groups. Further hydrolysis reactions eliminate Si and N atoms from the network, e.g. in the form of $Si(OH)_4$ and NH_3 which are dissolved in the aqueous medium. Internal and external corrosion can proceed by the same mechanisms.

If water, oxygen and ions can diffuse through the

passivation layer and reach metal sublayers (e.g. conducting tracks) corrosion of the metallic sublayer can occur. Depending on the adhesion strenghts between the layer systems this sublayer corrosion proceeds with or without delamination of the passivation layer.

Group 3 corrosion failures are related to the combined action of mechanical stress and chemical interactions and follow the mechanism of stress corrosion cracking. This type of corrosion mechanism has been intensively studied in recent years at silica glass and amorphous silica. The model today most widely accepted is based on the slow fracture Michalske–Freiman (MF) model and Michalske–Bunker (MB) model [55,56]. The MF-model involves a three step reaction sequence for water attack at strained Si–O–Si bonds existing either at the plain surface or at a crack tip (Fig. 5). In step 1 a water molecule is adsorbed at the strained Si–O–Si bond. This occurs via interaction of the oxygen lone electron pair on the water molecule with a silicon atom and hydrogen bond formation of a proton of the water molecule with the bridging oxygen atom. In step 2 the Si–O bond and the O–H bond in the adsorbed water cleave in a concerted action to form two hydrogen-bonded silanol groups. In step 3 the remaining hydrogen bond (which is expected to be weak if at all present) cleaves to leave fracture surfaces covered by silanol groups.

It could be shown that all molecules which (i) have at least one lone (nonbonding) electron pair (Lewis bases), (ii) possess a labile proton (Bronsted acid) and (iii) contain a distance between acid and base sites which conforms with the Si–O bond distance [55,56]. This holds except water also for ammonia [56]. Physisorbing molecules such as pyridine also adsorb on active sites but will not directly result in bond cleavage, instead it will block dissociatively adsorbing species from reaction [56]. This seems to open the possibility for inhibition of stress corrosion cracking at passivating amorphous films.

A good understanding of water-induced stress corrosion cracking of amorphous silica was obtained by a ring size distribution analysis in amorphous silica via molecular orbital calculations [57] considering a cluster of three-, four-, five- and six-membered silica rings. The cluster approximated the Bell–Dean distribution of three-, four-, five- and six-membered rings using 12 rings (Fig. 6). The concentration of the rings was 8, 17, 25 and 50%, respectively. The calculations showed that ring opening through hydrolysis is the lowest-energy pathway for water-enhanced fracture. While the theoretical strength of the Si–O bonds is greater than 100 kcal mol^{-1}, the barrier to fracture four-, five- and six-membered rings in the presence of water molecules was found to never exceed the +18 kcal mol^{-1} for a four-membered ring. The hydrolysis-induced fracture of a three-membered ring turned out to occur spontaneously at −3.6 kcal mol^{-1}. Crack propargation occurs by movement of a crack tip, i.e. a strained Si–O bond, through the amorphous silica structure. As the crack tip moves it will encounter all sorts of rings, mainly five- and six-membered rings and only very rarely a three-membered ring. In this manner the crack will be stopped or accelerated as it encounters different ring structures of different size [57].

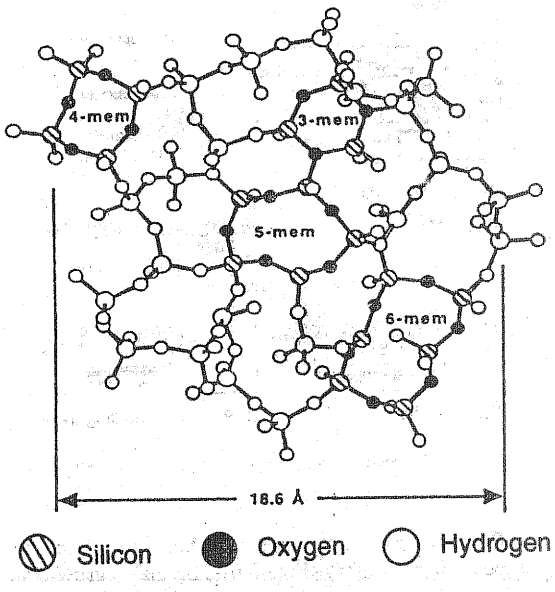

Fig. 6. Molecular mechanics structure of amorphous silica with Bell–Dean distribution of rings [57].

The stress corrosion mechanism proposed for amorphous SiO_2 should be analogously transferable on amorphous Si–N material. The mechanism underlines the importance of intrinsic stress in passivation layers and explains the fact that the thermal history and the processing greatly affects the cracking susceptibility of amorphous passivation layers.

3. Experimental

3.1. Microelectrode array

In order to study the long-term stability of passivation layers on sensor chips a versatile micro electrode array with different electrode shapes and sizes was developed (Fig. 7a). The design was intended to allow the investigation of the effect of various electrode geometries as well as different passivation materials on the kinetics of environmental degradation. On each sensor chip 14 rectangular electrodes with different sizes (10 × 10 to 200 × 200 μm^2) and two triangular electrodes (1.5 × 3.0 mm) were arranged.

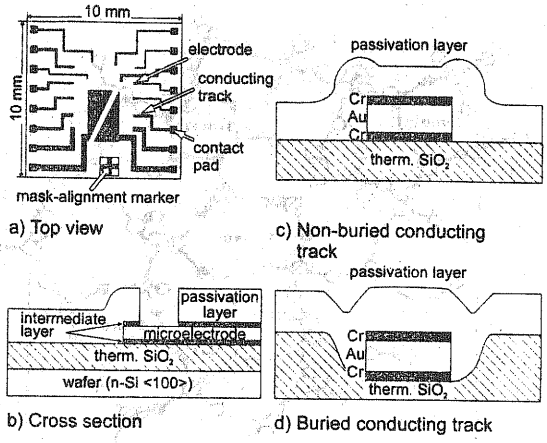

Fig. 7. Design structures of microelectrode array.

The microelectrode array was fabricated from low-doped silicon wafers (Fig. 7b). Thermally grown SiO_2 (270 up to 500 nm) was used as insulating material. As material for the electrodes and conducting tracks Au, Ag and Pt were deposited by vacuum evaporation with layer thicknesses between 200 and 400 nm. To improve the metallic adhesion, intermediate layers of Cr, Ni and Ti, respectively, were applied.

The passivation layers tested included inorganic and organic films. The inorganic layers were deposited by the PECVD process and included mono-layers (SiO_2 and Si_3N_4, respectively; thickness: 800 nm), duplex layers (400 nm SiO_2 capped with 400 nm Si_3N_4) and oxide-nitride-oxide (ONO) triplex layers (130 nm SiO_2 + 540 nm Si_3N_4 + 130 nm SiO_2). The organic passivation layers were applied by spin coating and included polyimide films (Selectilux HTR 3/Merck; thickness: 800 and 1000 nm, respectively) and novolack-based photoresist (AZ 5214/Hoechst; thickness: 1400 nm) [58].

To investigate the barrier effect of the passivation layers, the complete chip surface was coated with the passivation layer. Only the bond pads were opened to allow electrical contact to the conducting tracks and the electrodes underneath the passivation films. In a second series of tests the electrode surfaces were opened to study the adhesion of the films and their susceptibility to delaminate during exposure in the corrosion media.

The passivation layers were characterised by topographic measurements with a perthometer, with the microscope, SEM and XPS. Details are published in Ref. [59].

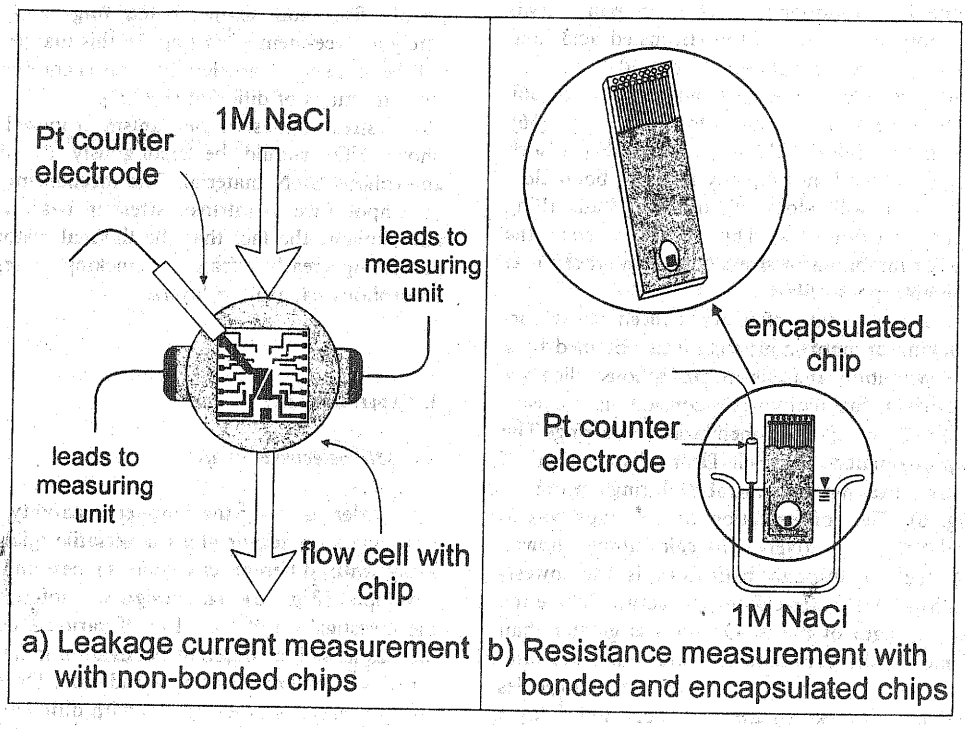

Fig. 8. Corrosion testing of passivation layers.

3.2. Corrosion media

The corrosion experiments were performed by exposing the chip in a flow cell or in an unstirred beaker at ambient temperature in aerated 1 M NaCl solution at pH values of 2, 7 and 10. The pH was adjusted either by adding dilute hydrochloric acid or sodium hydroxide solution.

3.3. Evaluation of experiments

Two kinds of experimental setup were used to evaluate the barrier effect of passivation layers. In the first series of experiments the chips were exposed in a flow cell (Fig. 8a). The volume of the test chamber was approx. 1 ml. The solution was slowly exchanged with a peristaltic pump. The flow cell was designed such that failed chips could be exchanged simply and quickly [58,60]. The electrical contact to the conducting tracks underneath the passivation layers was achieved by pressing rubber strips laminated with conductive layers onto the bond pads. The conducting layers were contacted with wires to measure each conducting track separately. Between the passivated conducting tracks (and the electrodes) and a platinum counter electrode in the corrosion medium a dc voltage of 1 V was installed. Failing of the passivation layer on a conducting track (with electrode) was monitored by measuring the level of the leakage current between the conducting track and the counter electrode. When the leakage current increased higher than 500 nA, the current signal indicated the time to failure to a PC.

In the second test series all microelectrodes were contacted via bond pads to a printed circuit board and encapsulated at the edges with a conventional epoxi resin (Fig. 8b). The surface of the passivation layer above the conducting tracks and the electrodes was left resin-free. The chip was dipped into the unstirred test solution and the time-related increase of the conductivity of the passivation layer between the conducting tracks and a platinum counter electrode was measured with a conductivity meter at 4 kHz and an ac voltage of 200 mV [61]. The increase of the conductivity indicated a degradation of the insulating properties of the passivation films. The time to failure of the passivation layer above a given conducting track (with electrode) was defined to be the time at which the film resistance decreased below 75 % of the initial resistance at the start of the experiment.

In order to identify the topography, the growth structure and the failure modes of passivation layers investigations were performed in the SEM.

4. Results and discussion

4.1. Fitness-for-purpose tests

The functionality of the microelectrode array was electrochemically tested by measuring cyclic voltammograms (CV) for all 16 opened gold electrodes in 0.5 M sulfuric acid at ambient temperature [58,62]. In Fig. 9a a set of CV curves of the differently sized gold microelectrodes are plotted in comparison to the CV of the triangular electrode. In this experiment, the potential range had to be limited to $U_{SHE} < 1.9$ V, since oxygen evolution attacks the passivation layer at the electrode edges.

The curves exhibit a slight deviation of the transferred charge in the anodic and the cathodic cycle

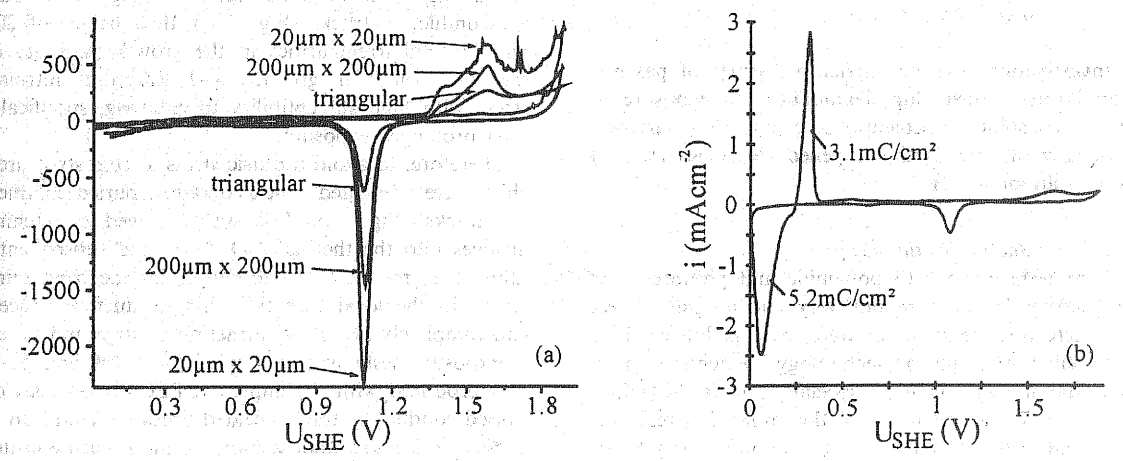

Fig. 9. Set of CV curves of different Au microelectrodes (a) and galvanic Cu deposition and dissolution on a 10×10 µm² Au electrode (b). Measuring conditions: 1 N H_2SO_4, $dU/dt = 50$ mV/s.

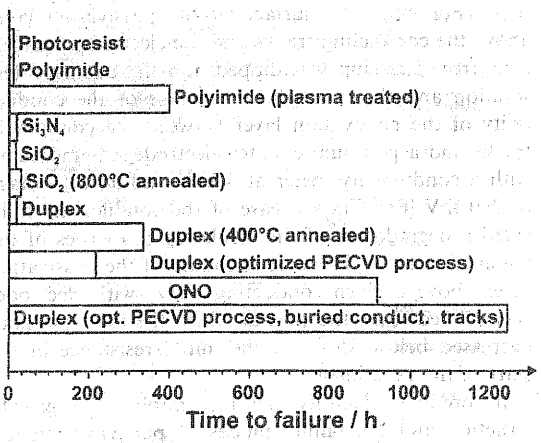

Fig. 10. Corrosion resistance of passivation layers in 1 M NaCl at 25°C.

which can be explained by the superposition of the oxygen generation during oxidation of the gold surface [63]. With decreasing size of the microelectrodes an increase of the current density was found. This is probably due to deviations of the theoretical from the actual electrode size as well as increased edge effects and contributions of the passivation material, which in this case was the duplex layer SiO_2/Si_3N_4.

It was further proved that the sensor array can be modified by galvanic depositing different metals (e.g. Cu, Ni, Pb) on top of the gold microelectrodes [59]. As an example, Fig. 9b presents a CV of a 10×10 μm^2 gold microelectrode in a Cu containing electrolyte. The CV depicts the Cu deposition in the cathodic cycle (0.1 V_{SHE}) and the Cu dissolution in the anodic cycle (0.3 V_{SHE}).

4.2. Corrosion testing

Investigations on the barrier properties of passivation layers against chip degradation on exposure to electrolyte solutions screening corrosion tests were performed with chips with unopened electrodes in 1 M NaCl solution at pH 7.

4.2.1. Organic passivation layers

First tests made with polyimide and photoresist as passivation layers were not very encouraging. These commercial grade materials were developed as masking materials for Si planar technology to achieve short-time stability against acids, specially HF. In 1 M NaCl with pH 7 delamination of the organic layers was observed at edges and steps and the protectivity lasted only a few hours (Fig. 10). However, by plasma surface treatment it was possible to improve the time to failure up to 400 h.

4.2.2. Inorganic passivation layers

In the as-deposited state the mono-layers of SiO_2 and Si_3N_4 and the duplex layer exhibited only poor protection (Fig. 10). The lowest time to failure showed the SiO_2 film (a few hours), while the plasma Si–N layer protected only for less than a day. Even the duplex layer failed already after one day.

As it is known that annealing can improve the barrier performance of PECVD deposits, all types of passivation layers were annealed for 10 minutes in an nitrogen atmosphere at temperature of 400 to 800°C. The plasma Si–N layer spalled already after annealing at 400°C due to high intrinsic stresses. Annealing at higher temperatures yielded an even higher spalling intensity.

SiO_2 layers could be annealed up to 800°C without spalling. The time to failure of such films was much higher (31 h) than in the as-deposited state (3 h).

The highest effect was observed when duplex layers were annealed for 10 min at 400°C. In this case the time to failure amounted to 340 h.

Very successful were attempts to improve the barrier properties of the duplex layers by modifying the PECVD deposition conditions. By decreasing the deposition rate a better growth structure with less intrinsic stress was obtained. This increased the time to failure of the as-deposited layers to 210 h.

The best results were obtained with the ONO triplex layer. Using the new modified conditions for the deposition of the intermediate plasma Si–N film, the protection of this passivation layer lasted nearly 1000 h (Fig. 10). The better performance of both duplex and ONO layers compared to monolayers of the same thickness is obviously due to the balancing of the counteracting intrinsic stresses in the SiO_2 and Si_3N_4 layers.

SEM investigations on the failure modes of the tested chips revealed that surface steps, e.g. at non-buried conducting tracks (Fig. 7c) with a height of 200 nm, induced irregularities in the growth structure of the films (nodular growth) and structural intrinsic stress with high susceptibility to cracking, specifically after prolonged exposure.

Therefore, to avoid intrinsic stress at step structures, chips were fabricated which contained buried conducting tracks (Fig. 7d). This was achieved by etching grooves into the thermal SiO_2 layer and subsequently filling the grooves with the deposit of the conducting track. In the ideal case this chip production process can completely avoid the formation of steps and edges.

Exposure tests with a duplex layer (plasma Si–N film produced with the improved PECVD process) on buried conducting tracks yielded times to failure up to 1250 h, i.e. more than 2 months, in the as-deposited state. Fig. 11a compares the time-related development of the relative resistance $R_{relative} = R/R_0$ (with R_0 being the resistance at time zero and R the resistance at a

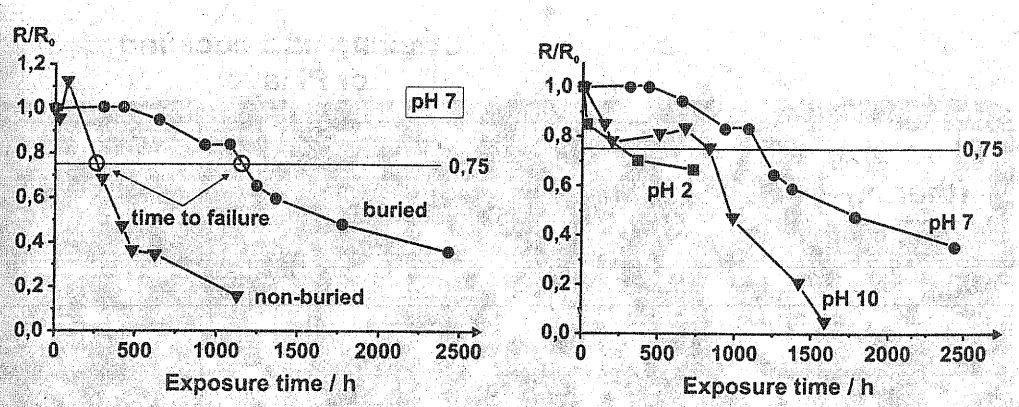

Fig. 11. Time development of the relative resistance R/R_0 of duplex layers in 1 M NaCl at 25°C.

given time) of chips with buried and non-buried conducting tracks during exposure in 1 M NaCl/pH 7 at ambient temperature. The time needed to reduce the film resistance to 75% of R_0 was defined as the time to failure.

Further experiments at pH 10 and pH 2 revealed that duplex layers (prepared with the improved deposition process and tested without any post-treatment) on chips with buried conducting tracks exhibit also considerable corrosion protectivity in mild basic and acid media (Fig. 11b). Typically, the performance is highest at pH 7 and the protection is better at pH 10 (800 h) than at pH 2 (300 h). This can be explained by considering the potential distribution across the interface (Fig. 12). The conditions are similar to those at passive films on metals, e.g. in the system $Hf/HfO_2/H_2O$ [64].

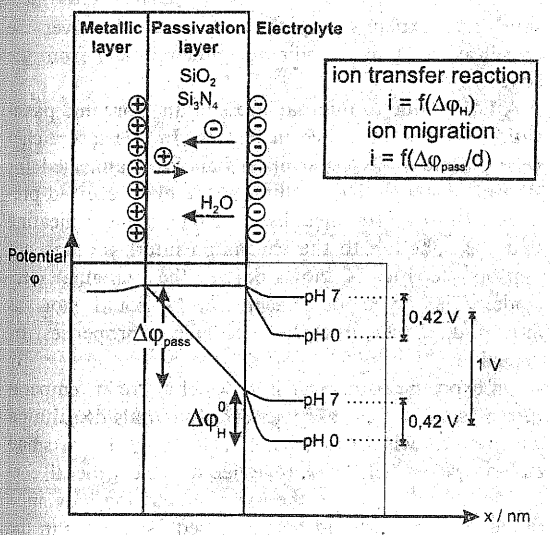

Fig. 12. Potential gradient at passivation layer affecting the ion migration and ion transfer reactions.

The total potential drop is given by

$$\Delta\varphi = \Delta\varphi_{m/pass} + \Delta\varphi_{pass} + \Delta\varphi_H \quad (4)$$

the potential drop at the interface oxide (or nitride)/water depends on the protolytic equilibrium and is usually given by

$$\Delta\varphi_H = \Delta\varphi_H^0 - \frac{2.3 \times RT}{F}\text{pH} \quad (5)$$

The potential drop in the passive layer $\Delta\vartheta_{pass}$ is linear, if there is no space charge. Otherwise a space charge layer has to be considered. Ion transfer reactions, e.g. the dissolution reaction of the oxide or nitride, will depend on the pH. Protolytic reactions and transfer of cations into the solution increase with decreasing pH, which is usually observed for the dissolution of oxides. On the other hand, complexation by OH^- ions enhances also the dissolution and corrosion may increase in alkaline solutions, too. Thus, the finding of maximum corrosion stability in neutral solutions is reasonable.

The results outlined above, which were obtained with chips completely covered with passivation layer (electrode surfaces not opened), clearly indicate that the barrier properties of passivation systems against corrosive deterioration can be optimised significantly.

The next step was to test chips with opened, non-buried electrode surfaces. It appeared that the performance of the optimised duplex layers was lower under these conditions due to delamination. However, using buried electrode surfaces delamination should be reduced considerably. This subject will be investigated further.

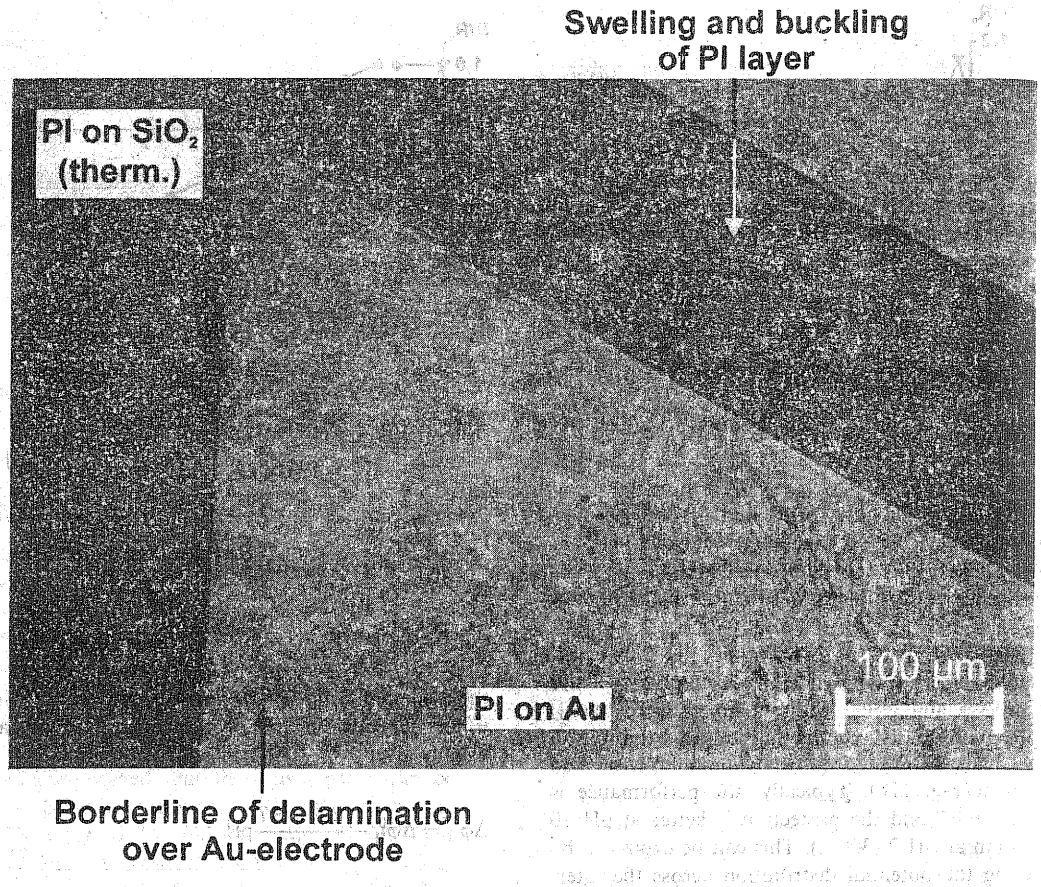

Fig. 13. Swelling and buckling of polyimide (Pl) film, predominantly on thermal SiO_2 layer.

4.3. SEM investigation of failure modes

The typical failure mode of *organic* passivations layers was water absorption with subsequent swelling and formation of blisters. Fig. 13 gives an example of a polyimide films which failed after 12 days in neutral 1 M NaCl solution at room temperature. It was found that blistering, buckling and delamination of the polyimide film started always on surface areas where the film was directly contacted with the thermal silica layer. Only at a later stage polyimide films showed blistering also over the gold conducting tracks. Detailed investigations proved that the delamination on the metallised surface areas started from the edges of the metallisation. It is assumed that blistering, delamination and buckling of polyimide films over thermal silica is due to osmosis. Diffusion of water through the polyimide film to hydrolysable centers on the silica surface and formation of hydrated or dissolved silicic acid at the interface produces a water concentration gradient which is the driving force for enhanced water diffusion. This explains why the polyimide film over the metallised areas is delaminated preferentially from the edges.

A failure due to internal stress in an inorganic passivation layer is illustrated in Fig. 14. In this case a chip with plasma Si–N passivation had been annealed for 10 min at 400°C. The spalling of the film occurred preferentially over the metallised surface areas indicating that the adhesion to the chromium interlayer was not appropriate. Fig. 14 shows part of the triangular electrode. This type of plasma Si–N could not be improved in its fracture mechanical properties by annealing.

On exposure to neutral 1 M NaCl at room temperature plasma Si–N films experience materials dissolution which starts with formation of a high density of small etching pits which grow together to yield general corrosion. Fig. 15 shows the state of etching pits in a duplex layer which had been exposed for 1100 h in the neutral electrolyte solution. Breaking the chip in liquid nitrogen revealed the structure and thickness of the

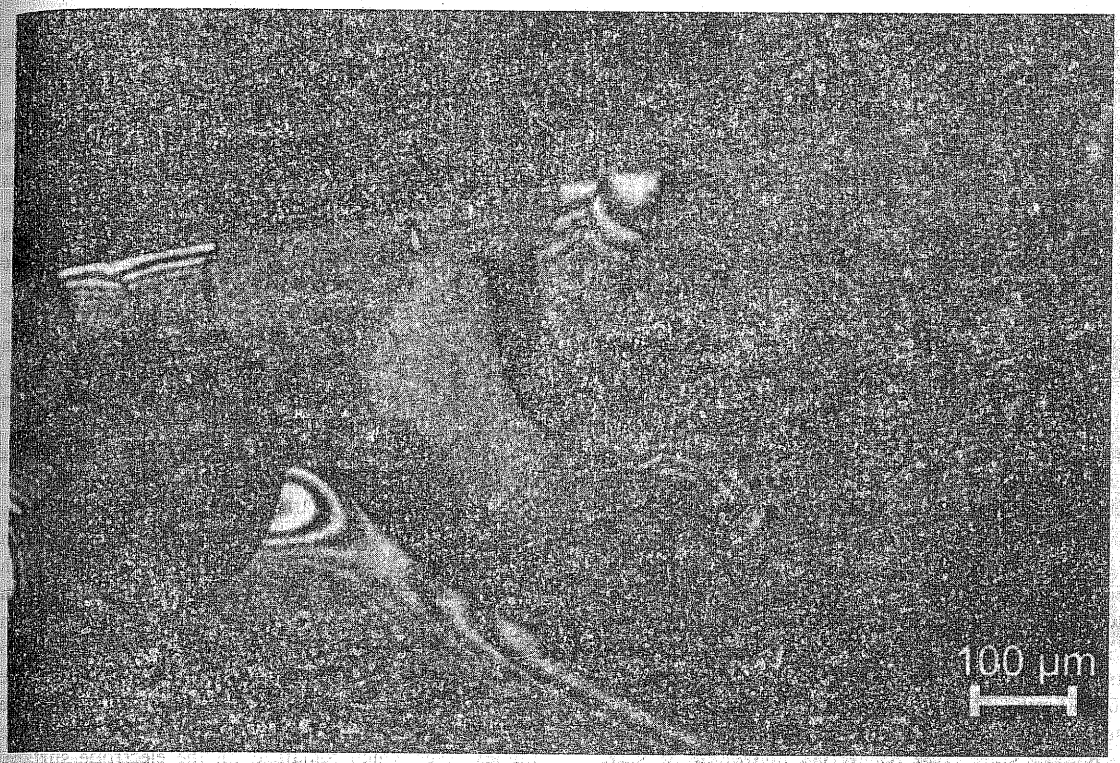

Fig. 14. Spalling of plasma Si–N layer due to intrinsic stress after annealing at 400°C (10 min) (no electrolyte exposure).

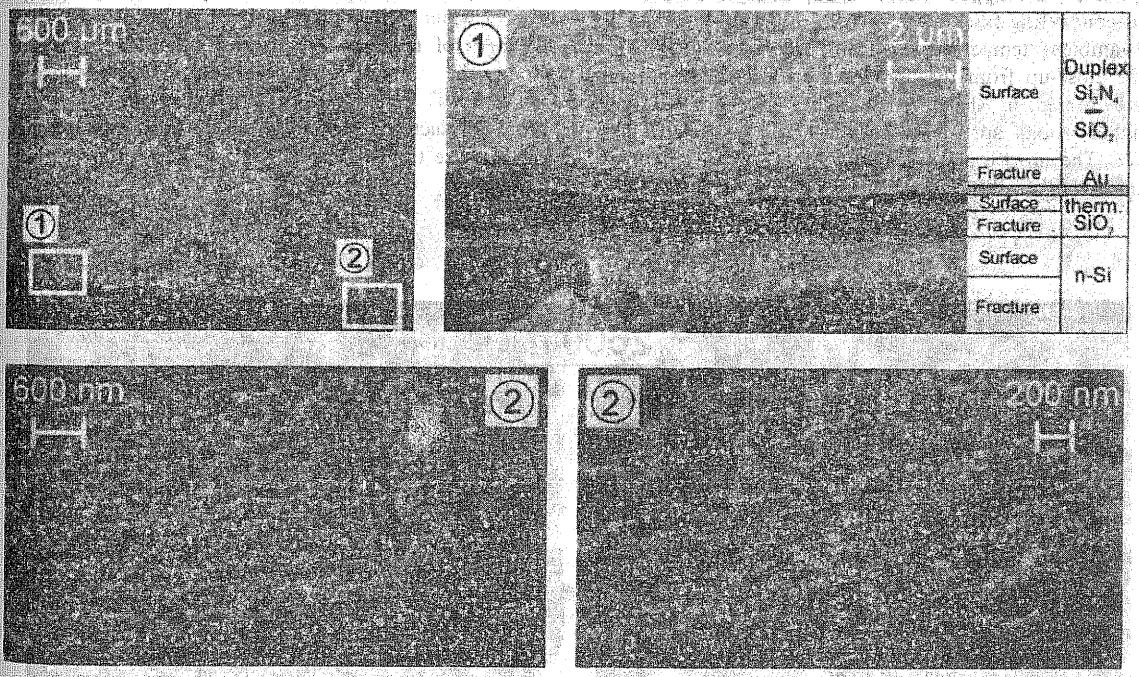

Fig. 15. Duplex passivation after 1100 h in 1 M NaCl at 25°C. Deliberate fracture through chip for fracture surface studies.

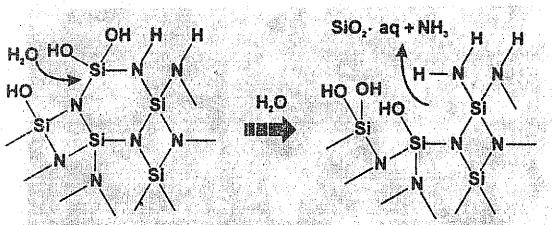

Fig. 16. Hydrolytic dissolution of plasma Si–N.

different layers on the chip. The magnification at site 1 shows the sequence of the different layers at the edge of a triangular electrode which had not been opened and is, therefore, still covered with the duplex layer. It was not possible to distinguish between the two types of plasma layers in the crack surface of the duplex layer. At the edge of the metallisation the typical nodular growth of the plasma-deposited duplex layer can be observed. A close-up of such nodular growth at step structures here after 1100 h corrosion gives the low left picture in Fig. 15, which was made from site 2. The low right picture demonstrates that the etching pits have an opening of 100–200 nm and a depth of 100–150 nm. This corresponds to a local corrosion rate of 0.1–0.2 nm/day. The chemical dissolution of the plasma Si–N layer occurs via hydrolysis of Si–N bonds and formation of silicic acid and ammonium hydroxide (Fig. 16).

The surface appearance of a duplex layer on a buried conducting track after 2600 h in neutral 1 M NaCl at ambient temperature is demonstrated in Fig. 17. The close-up from the corner of an electrode, in this case buried in the thermal silica layer, shows the slightly rough surface of the generally corroded surface. The groove at the edge of the electrode and the conducting track was caused by the fact that the etch groove in the thermal silica layer had been a little wider than the diameter of the conducting track due to isotropic etching with diluted HF.

Nevertheless, the long lasting barrier effect (more than 1250 h, i.e. nearly two months) of the duplex layer on buried conducting tracks and electrodes clearly demonstrates that minimising or avoiding topographically induced intrinsic stresses at step structures is an important necessity to produce microelectrode sensor arrays with high service life under corrosive environmental conditions. If layer imperfections like pinholes or particle inclusions (Fig. 18) are avoided, even longer corrosion protection can be achieved with optimised chip design and improved plasma deposition process of the passivation layer.

Optimised chips will have buried conducting tracks and electrodes. Under these conditions the risk of delamination of the passivating layer will be considerably lower, even in case of opened electrodes. On chips with classical non-buried conducting tracks and with opened electrodes delamination of the passivation film was observed after longer exposure times (1350 h) in neutral 1 M NaCl at ambient temperature (Fig. 19a, b and c). The delamination started at the overlay on the electrode and progressed to the conducting tracks. The close-up in Fig. 19c clearly shows that the rest of the duplex layer which remained on the electrode surface, buckled and cracked in the corner. This indicates that the layer contained intrinsic compressive stresses which probably increased due to swelling caused by absorption of water. The cracks occurred in the corner, i.e. in the area of highest stress intensity. Uptake of water along the interface metallisation/plasma deposited silica stimulates the progress of delamination via hydrolysis reactions. Fig. 19d shows the as-deposited state before the exposure. No cracks and buckling are visible.

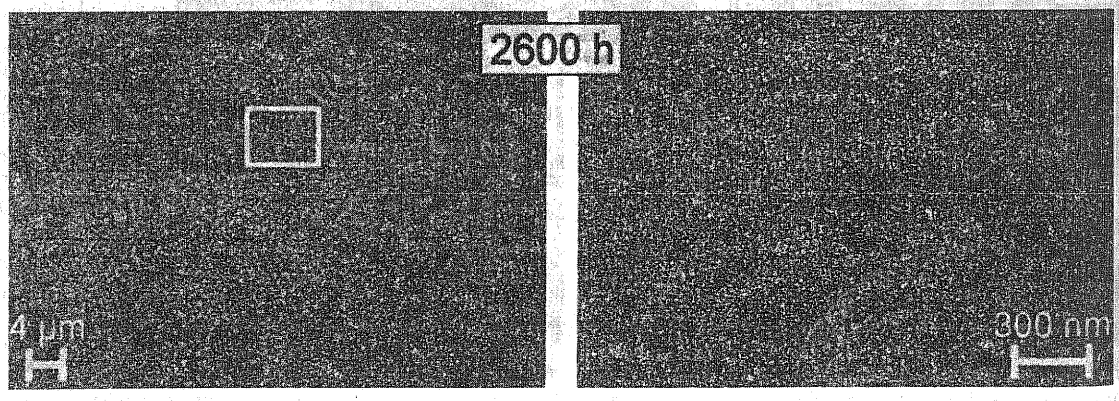

Fig. 17. Duplex passivation on buried conducting tracks after 2600 h in 1 M NaCl at 25°C.

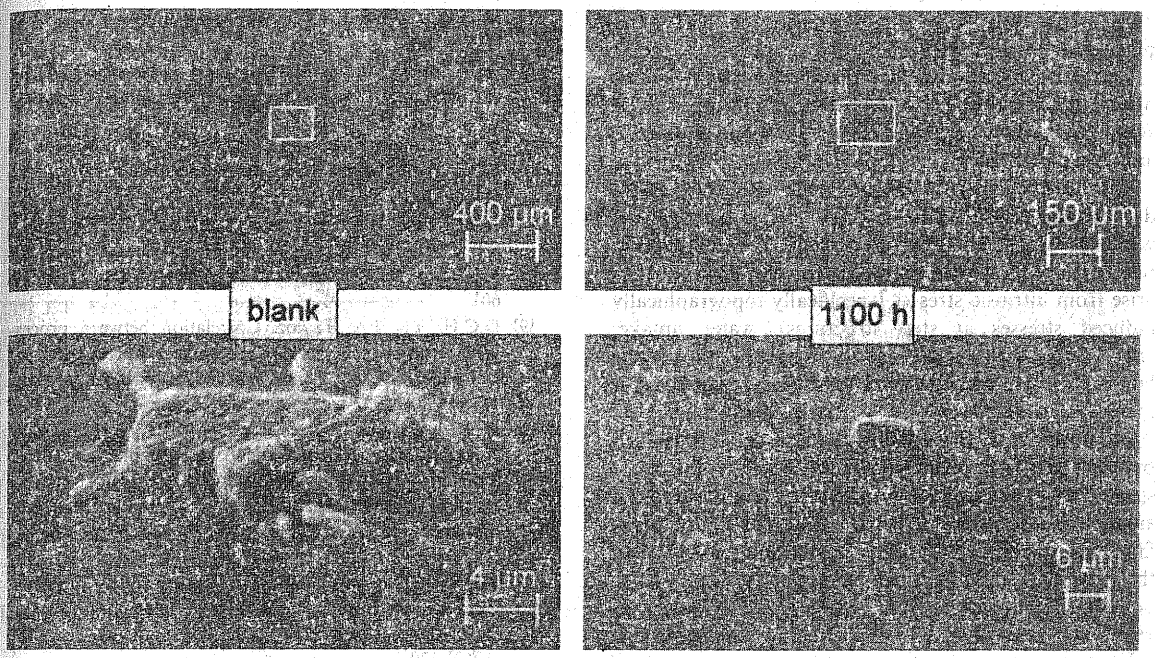

Fig. 18. Particle inclusions in duplex passivation layer.

5. Conclusions

The barrier performance of passivation layers to prevent corrosion of sensor chips can be optimised by the chip design, the appropriate selection of the type of passivation layer and by optimising the deposition conditions. Organic passivation layers like photoresist or polyimide suffer from water absorption with subsequent swelling, delamination and formation of blisters. The time to failure was in the range of a few

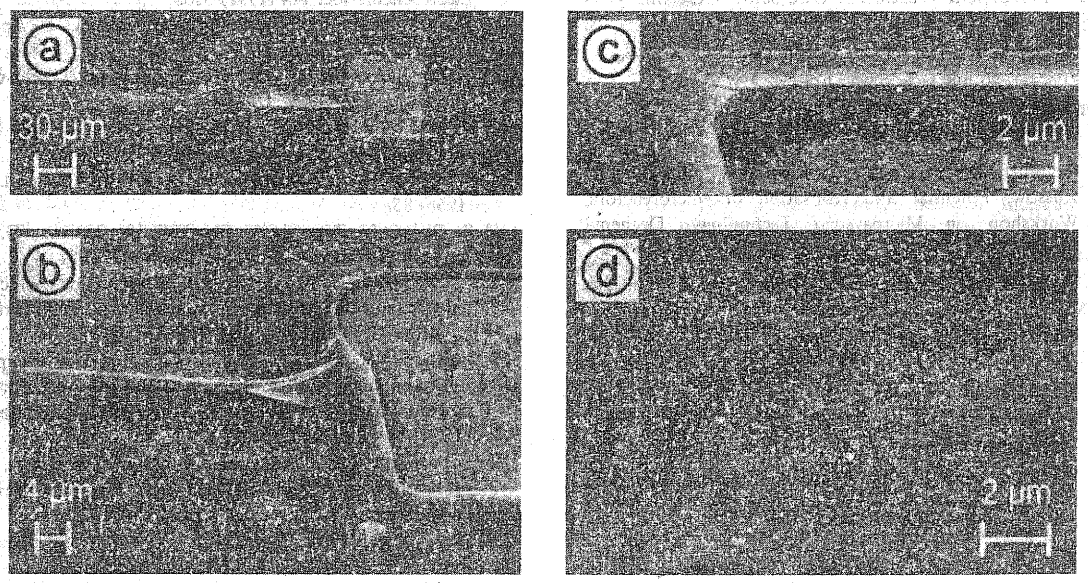

Fig. 19. Delamination of duplex passivation layer on non-buried conducting track and opened Au electrode after 1350 h in 1 M NaCl at 25°C (a, b and c). For comparison: opened electrode before exposure (d).

hours. However, it can be increased to 400 h by plasma surface treatment.

Inorganic passivation layers exhibit a much higher optimisation potential, e.g. by optimising the deposition process and the post-deposition conditions, e.g. annealing conditions.

The best results were obtained with SiO_2/Si_3N_4 duplex and $SiO_2/Si_3N_4/SiO_2$ (ONO) triplex layers, which gave protection for more than 1200 and 1000 h, respectively. However, problems for the film integrity arise from intrinsic stresses (specifically topographically induced stresses at step structures), water uptake, cracking and delamination. They can be minimised by burying the conducting tracks in the insulating layer of thermal SiO_2.

Impairments of the passivation film can be observed by SEM or by decoration with cathodic metal deposition [59]. Experiments proved that the stability of amorphous, non-stoichiometric plasma Si–O and Si–N films in aqueous solutions is significantly lower than the corresponding stoichiometric crystalline compounds. Reactions at the surface and diffusion of water and electrolyte into the film play an important role.

Acknowledgements

This work was performed within the joined research program "Integrated Microsystem Technology for Solid/Liquid Systems". Financial support by the Ministerium für Wissenschaft und Forschung des Landes Nordrhein-Westfalen, Düesseldorf/Germany, is gratefully acknowledged.

References

[1] W. Ehrfeld, V. Hessel, H. Moebius, Th. Richter, K. Russow, Potential and realisation of microreactors, Workshop on Microsystem Technology, Dechema Monographs, vol. 132, Mainz (20-21 February), 1995.

[2] A. Uhlig, M. Paeschke, K. Schakenberg, R. Hintsche, H.-J. Diederich, F. Scholz, Chip-array electrodes for stripping analysis of trace metals, Sensors Actuators B 24–25 (1995) 899.

[3] W. Goepel, J. Hesse, J.N. Zemel, in: Sensors: a Comprehensive Story, vols. 2–3, VCH Verlag, Weinheim, 1996.

[4] U. Wollenberger, R. Hintsche, F. Scheller, Biosensors for Analytical Microsystems, Microsyst Technol 1 (1995) 75.

[5] W.A.P. Claassen, W.G.J.N. Valkenburg, M.F.C. Willemsen, W.M. v.d. Wijgert, Influence of deposition temperature, gas pressure, gas phase composition and rf frequency on composition and mechanical stress of plasma silicon nitride layers, J. Electrochem. Soc. 132 (1985) 893.

[6] G. Kelm, G. Jungnickel, Hydrogen in plasma enhanced chemical vapor deposition insulating films, Mater. Sci. Eng. A 139 (1991) 401.

[7] W.A. Lanford, M.J. Rand, The hydrogen content of plasma-deposited silicon nitride, J. Appl. Phys. 49 (1978) 2472.

[8] A.K. Sinha, H.J. Levinstein, T.E. Smith, G. Quintana, S.E. Haszko, Reactive plasma deposited Si–N films for MOS-LSI passivation, J. Electrochem. Soc. 125 (1978) 601.

[9] D.C.H. Yu, J.A. Taylor, Correlation between processing, composition and mechanical properties of PECVD-SiN_x Thin Films, Mater. Res. Soc. Symp. Proc. 188 (1990) 1202.

[10] R. Srinivasan, B.C. Nguyen, A.P. Short, Plasma enhanced chemical vapor deposition of dielectric films: correlation of stress to film structure and plasma characteristics, Mater. Res. Soc. Symp. Proc. 188 (1990) 101.

[11] W. Kern, G.L. Svchnable, A.W. Taylor, RCA Rev. 37 (1976) 3.

[12] P.M. Schiable, R. Glang, in: F. Vratny (Ed.), Thin Film Dielectrics, Electrochemical Society, New York, 1969.

[13] R. Lathlaen, D.A. Diehl, J. Electrochem. Soc. 116 (1969) 620.

[14] H. Sankur, W. Gunning, J. Appl. Phys. 66 (1989) 807.

[15] W.A. Pliskin, J. Vac. Sci. Technol. 14 (1977) 1064.

[16] J. Wong, J. Electron Mater. 5 (1976) 113.

[17] A.C. Adams, F.B. Alexander, C.D. Capio, T.E. Smith, J. Electrochem. Soc. 128 (1981) 1545.

[18] T.H. Tom Wu, R.S. Rosler, Stress in PSG and nitride films as related to film properties and annealing, Solid State Technol. 65 (May 1992).

[19] M.S. Haque, H.A. Naseem, W.D. Brown, J. Electrochem. Soc. 144 (1997) 3265.

[20] M.S. Haque, H.A. Naseem, W.D. Brown, J. Appl. Phys. 82 (1997) 2922.

[21] W.A. Pliskin, R.M. Valetta, IBM Techn. Disclosure Bull. 10 (1967) 490.

[22] W. Kern, RCA Rev. 37 (1976) 55.

[23] W. Kern, J. Electrochem. Soc. 116 (1969) 251C.

[24] W.A. Pliskin, P.P. Castrucci, Electrochem. Technol. 6 (1968) 85.

[25] S. Rojas, L. Zanotti, A. Borghesi, A. Sassalla, G.U. Pignatel, J. Vac. Sci. Technol. B 11 (1993) 2081.

[26] J.N. Cox, in: V.J. Kappoor, W.D. Brown (Eds.), Silicon Nitride and Silicon Oxide Thin Insulating Films, Proc. 14–16, ECS, Pennington, NJ, 1994, p. 117.

[27] M.S. Haque, H.A. Naseem, W.D. Brown, Post-deposition processing of low temperature PECVD silicon dioxide films for enhanced stress stability, Thin Solid Films 308–309 (1997) 68–73.

[28] D.L. Smith, A.S. Alimonda, C.C. Chen, S.E. Ready, B. Wacker, Mechanism of SiN_xH_y deposition from NH_3–SiH_4 plasma, J. Electrochem. Soc. 137 (1990) 614.

[29] A.K. Sinha, H.J. Levinstein, The Electrochemical Society, Fall Meeting, Las Vegas, Nevada (Oct. 17–22, 1976), Abstracts 242 and 244, pp. 625, 626, 629 and 630.

[30] A.K. Sinha, H.J. Levinstein, T.E. Smith, Thermal stress

and cracking resistance of dielectric films (SiN, Si_3N_4, SiO_2)on Si substrates, J. Appl. Phys. 49 (4) (1978) 2423.
[31] W.A.P. Claassen, W.G.J.N. Valkenburg, F.H.P.M. Habraken, Y. Tamminga, J. Electrochem. Soc. 130 (1983) 2419.
[32] A.K. Sinha, H.J. Levinstein, T.E. Smith, G. Quintana, S.E. Haszko, J. Electrochem. Soc. 125 (1978) 601.
[33] T.F. Retajczyk, A.K. Sinha, Thin Solid Films 70 (1980) 241.
[34] F.H.P.M. Habraken, A.E.T. Kuiper, A. v. Oostrom, Y. Tamminga, J.D. Theeten, J. Appl. Phys. 53 (1982) 404.
[35] E.P. Eernisse, J. Appl. Phys. 48 (1977) 3337.
[36] K. Allaert, A. van Calster, H. Loos, A. Lequesue, A comparison between silicone nitride films made by PCVD of N_2–SiH_4/Ar and N_2–SiH_4/He, Solid-State Sci. Technol 132 (1985) 1763.
[37] W.-S. Liao, C.-H. Lin, S.-H. Lee, Oxidation of silicon nitride prepared by plasma-enhanced chemical vapour deposition at low temperature, Appl. Phys. Lett. 65 (17) (1994) 2229.
[38] E.S. Kim, J.R. Kim, R.S. Muleer, Improved IC-compatible piezoelectric microphone and CMOS process, Transducers '91, Digest Techn. Papers, p. 270.
[39] P.V. Pavlow, E.V. Shitova, E.I. Zorin, N.A. Genkina, Crystallisation of amorphous films of silicon nitride by ionic bombardment followed by annealing, Sov. Phys.-Crystallogr. 18 (1973) 381–383.
[40] A. Stoffel, A. Kovács, W. Kronast, B. Mueller, LPCVD against PECVD for micromechanical applications, J. Micromech. Microeng. 6 (1996) 1.
[41] D. Maier-Schneider, J. Maibach, E. Obermeier, in: Computer-aided characterization of the elastic properties of thin films, MME '92, 3rd European Workshop on Micromachining, Micromechanics and Microsystems, Leuven, 1992, p. 90.
[42] S. Sugiyama, K. Shimaoka, O.Tabata, Surface micromachined microdiaphragm pressure sensors, Transducers '91, Digest Techn. Papers, p. 188.
[43] S.M. Sze, VLSI Technology, McGraw-Hill, New York, 1988.
[44] P.R. Scheeper, J.A. Voorthuysen, P. Bergveld, PECVD silicon nitride diaphragms for condenser microphones, Sensors Actuators B 4 (1991) 79.
[45] H. Dun, P. Pan, F.R. White, R.W. Douse, Mechanism of plasma-enhanced silicon nitride deposition using SiH_4/N_2 mixture, Solid State Sci. Technol. 128 (1981) 1555.
[46] G.M. Samuelson, K.M. Mar, The correlations between physical and electrical properties of PECVD SiN with their composition ratios, Solid State Sci. Technol. 129 (1982) 1773.
[47] K. Aite, J. Hollemann, J. Middlekoek, R. Koekoek, The relationship between intrinsic stress of silicon nitride films and ion generation in a 50 kHz RF discharge, in: SO Thin Films, Stresses and Mechanical Properties Symp., Materials Research Society, Boston, MA; Pittsburg, PA, 1988.
[48] R.S. Wagner, W.C. Ellis, Trans. AIME 223 (1965) 1053.
[49] W. Kern, R.S. Rosler, J. Vac. Sci. Technol. 14 (1977) 1082.
[50] R. Robertson, M.I. Manning, Mater. Sci. Techn. 6 (1990) 81.
[51] R.K. Ulrich, W.D. Brown, S.S. Ang, S. Yi, J. Sweet, M.D. Peterson, PECVD silicon nitride postbond films for protecting bondpads, bonds and bondwire from corrosion failure, IEEE 0569–5503 (1991) 738.
[52] K. Dyrbye, T. Romedahl-Brown, G.F. Eriksen, Packaging of physical sensors for aggressive media applications, J. Micromech. Microeng. 6 (1996) 187–192.
[53] J.V. Dalton, J. Drobek, J. Electrochem. Soc. 115 (1969) 865.
[54] M.T. Duffy, W. Kern, RCA Rev. 31 (1970) 742.
[55] T.A. Michalske, S.W. Freiman, A molecular mechanism for stress corrosion in vitreous silica, J. Am. Ceram. Soc. 66 (1983) 284–288.
[56] T.A. Michalske, B.C. Bunker, J. Appl. Phys. 56 (1984) 2686.
[57] J.K. West,L, L. Hench, Philos. Mag. A 77 (1998) 85.
[58] A. Riemer, G. Buss, J.W. Schultze, M.J. Schöning, A. Steffen, P. Kordos, H. Lüth, Silicon-based microelectrode array for research and development, Electrochim. Acta, submitted for publication.
[59] G. Buß, M.J. Schöning, H. Lüth, J.W. Schultze, Modifications and characterisations of a silicon-based microelectrode array, Electrochim. Acta, submitted for publication.
[60] C. Haan, Diploma thesis, Aachen University of Technology. Aachen, 1996.
[61] F. Faßbender, Ph.D. thesis, Aachen University of Technology, Aachen, presum. 1999.
[62] M.J. Schöning, G. Buß, F. Faßbender, O. Glück, G. Schmitt, J.W. Schultze, H. Lüth, A silicon-based microelectrode array for chemical analysis, in: Proc. 7th Intern. Meeting on Chemical Sensors, International Acad. Publishers, Beijing, China, 1998, p. 100.
[63] D. Dickertmann, J.W. Schultze, K.J. Vetter, Electrochemical formation and reduction of monomolecular oxide layers on (111) and (100) planes of gold single crystals, Electroanal. Chem. 55 (1974) 429.
[64] C. Bartels, J.W. Schultze, U. Stimming, M.A. Habib, Electrochim. Acta 27 (1982) 129.